

Rotational Variability and Detection of Superflares in a Young Brown Dwarf by TESS

Rajib KUMBHAKAR*, Soumen MONDAL*, Samrat GHOSH, Diya RAM
and Sudip PRAMANIK

S. N. Bose National Centre for Basic Sciences, Salt Lake, Kolkata 700106, India

* Corresponding authors: rajskbuph0@gmail.com; soumen.mondal@bose.res.in

This work is distributed under the Creative Commons CC-BY 4.0 Licence.

Paper presented at the 3rd BINA Workshop on “Scientific Potential of the Indo-Belgian Cooperation”, held at the Graphic Era Hill University, Bhimtal (India), 22nd–24th March 2023.

Abstract

We present a comprehensive analysis of a Transiting Exoplanet Survey Satellite (TESS) high-quality light curve for a young brown dwarf, MHO 4 having spectral type M7.0, in the Taurus star-forming region. We investigate the rotation periods and characterize the brown dwarf’s dynamic atmosphere and surface features. Our light curve analysis of MHO 4 reveals a rotation period of approximately 2.224 days. Remarkably, MHO 4 exhibits two significant flaring events. Furthermore, we estimate the bolometric flare energies to be within the energy range of 10^{34} to 10^{35} erg, classifying them as superflares.

Keywords: brown dwarfs, TESS, photometric variability, periodic variables, starspots

1. Introduction

Brown dwarfs (BDs) were initially theorized by Shiv Kumar in 1962 (Joergens, 2014), and since then, thousands of BDs have been discovered (Martín et al., 1999; Carnero Rosell et al., 2019). BDs occupy an intermediate-mass range between planets and stars, typically ranging from approximately 13 to 80 times the mass of Jupiter. Due to their low masses, they cannot sustain nuclear fusion by burning hydrogen inside their core; instead, they burn deuterium. Being cool and fully convective, BDs show different kinds of atmospheric features and cause flux modulation as they rotate, which can be interpreted by studying the light curve. Therefore, photometric variability is an important tool for studying their surface characteristics and atmospheric properties.

In recent years, variability of these objects has been observed over a broad range of wavelengths (Carpenter et al., 2001; Ghosh et al., 2021; Wang et al., 2023). In the optical range, photometric variability of BDs mainly arises due to the rotational modulation of active starspot regions in the photosphere, along with magnetically induced chromospheric activity at higher altitudes in the atmosphere, dust clouds, or binary companions. Thus, variability can probe the diverse set of several physical mechanisms for these classes of young objects and study

diverse environments. With age, the shape of light curves of young objects, their rotation periods, and surface features in the photosphere have been investigated by the availability of high-cadence and high-precision photometric observations from spacecraft such as CoRoT (Baglin et al., 2006), MOST (Matthews et al., 2000), and the *Kepler* extended mission K2 (Howell et al., 2014). Here, we used the Transiting Exoplanet Survey Satellite (TESS; Ricker et al., 2015), which also provides high-cadence, high-precision light curves of young objects, covering many young clusters, including the extended Taurus star-forming region with a wavelength range from 600 to 1000 nm.

In this study, we present the analysis of TESS photometric data of a young BD, MHO 4 (TIC 456944264), with spectral type M7.0 (White and Basri, 2003). It is a bona fide member of the young Taurus star-forming region. We further analyze the power spectrum to infer the rotation periods and the physical mechanism behind stellar flares. Section 2 describes the TESS observation and data analysis procedure, including period analysis. In Sect. 3, we present the light curve of our source and describe flare analysis and the results derived from them. Finally, in Sect. 4, we summarize the key findings of our study.

2. TESS Observations and Data Analysis

We used the time-series data of TESS, briefly discussed here (for more details, please see Ricker et al., 2015). TESS is a space-based telescope launched by NASA in April 2018. It comprises four cameras with a size of 10 cm and a combined field of view $24^\circ \times 96^\circ$. During the first extended mission, TESS observed our selected object, MHO 4, in both TESS sector 43 (Camera 3 and CCD 3) and sector 44 (Camera 2, CCD 4). We employed 2-min cadence photometry, which is publicly accessible through the Mikulski Archive for Space Telescopes (MAST). We used the `lightkurve` (Lightkurve Collaboration et al., 2018) package to download the light curve of MHO 4 from MAST. These data had already been processed by the Science Processing Operations Center (SPOC), and we used the Pre-search Data Conditioning Simple Aperture Photometry (PDCSAP) flux for our analysis. PDCSAP light curves are generated from the SAP flux, which are removed of systematic effects using the Pre-search Data Conditioning (PDC) pipeline module (for more details, see Jenkins et al., 2016). Additionally, we utilize the ‘hardest’ bitmask filter in `lightkurve` and then filtered the data by removing outliers and NaN values. We further normalized the light curves by dividing each flux by its mean.

Visual inspection of the PDCSAP light curve of MHO 4 in Fig. 1 reveals a variable nature across the sectors. Additionally, Fig. 1 also shows the periodogram and phase folded light curve of MHO 4.

Here, we utilized two independent techniques to deduce the rotation period of MHO 4 using TESS data: the Lomb–Scargle periodogram (VanderPlas, 2018) and the Gaussian Process (GP; Angus et al., 2018). The `lightkurve` periodogram was utilized to estimate the object’s period, and the phase curve was constructed using the most significant peaks in the periodogram. Additionally, we attempted to infer the rotation period using the GP method and provided a posterior probability distribution function, which can be used to estimate the uncertainty in the

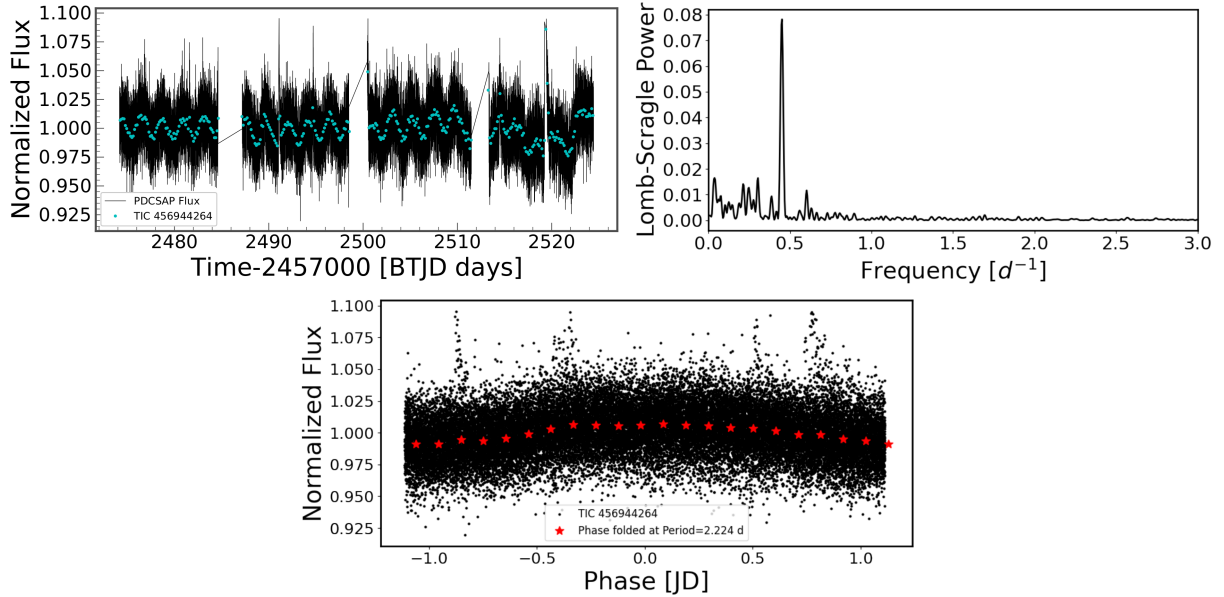


Figure 1: The TESS PDCSAP light curve (*top left*), LS periodogram (*top right*) and phase folded light curve (*bottom*) of MHO 4 are shown. Blue dots in the light curve represent the binning points of 200 min and red dots are the 150-min binning points in the phase curve.

rotation periods. Furthermore, for the GP method, we used the `exoplanet` (Foreman-Mackey et al., 2021) and `celerite2` (Foreman-Mackey, 2018) packages to model rotation periods in each sector individually. We opted to use the `PyMc3` package for the posterior distribution as it offers various general models. The estimated rotation periods of MHO 4 from TESS 2-min cadence data are described in Sect. 3. Furthermore, the `Allesfitter` code is utilized to model the detected complex flare events of MHO 4 via Bayesian evidence.

3. Results and Discussion

MHO 4 is a young BD of spectral type M7.0, with $T_{\text{eff}} = 2814$ K and $R = 0.655R_{\odot}$ (Stassun et al., 2018), belonging to the Taurus association. Previously, Briceño et al. (1998) identified strong absorption lines, including Li I $\lambda 6707$, He I $\lambda 5876$, [O I] $\lambda 6300$, and [O I] $\lambda 6363$, for this object. Rebull et al. (2020), using K2 observation, reported a period of approximately 2.2098 d, while Güdel et al. (2007) recorded an upper limit of the rotation period as 6.29 d based on X-ray observation with the *XMM-Newton* data. Figure 1 illustrates the TESS light curve, LS periodogram, and phase curve of MHO 4 stitched across both sectors. We measured the rotation period using the LS method to be 2.224 d, and when analyzing each TESS sector separately, we also obtained consistent periods. The estimated rotation period using the GP method is $2.215^{+0.017}_{-0.016}$ d in sector 43 and $2.205^{+0.047}_{-0.043}$ d in sector 44. The rotation periods derived from these two independent methods exhibit reasonably close values. The posterior distribution of rotation periods of MHO 4 for both sectors are shown in Fig. 2.

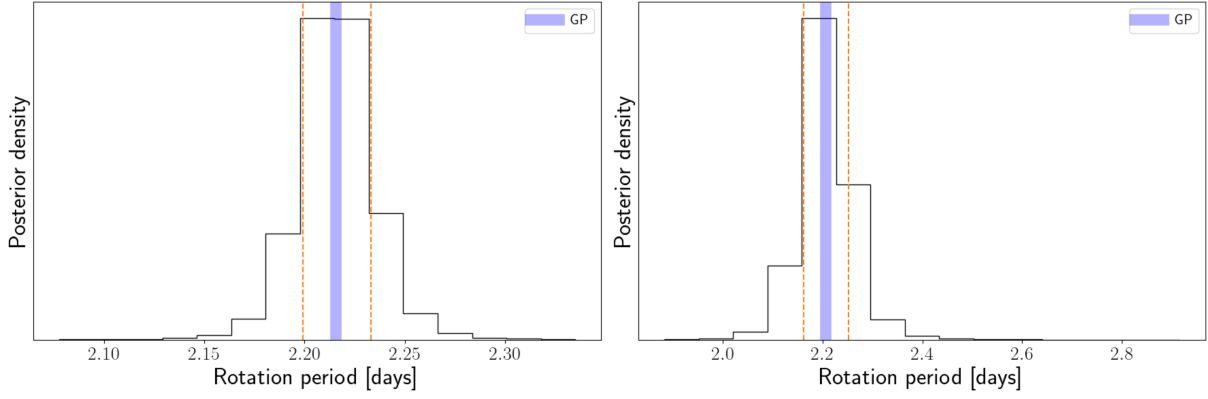


Figure 2: Posterior models of rotation periods of MHO 4, measured from TESS 2-min cadence data in sector 43 (*left*) and sector 44 (*right*). The blue line represents the rotation periods and the orange lines are the uncertainties of the periods.

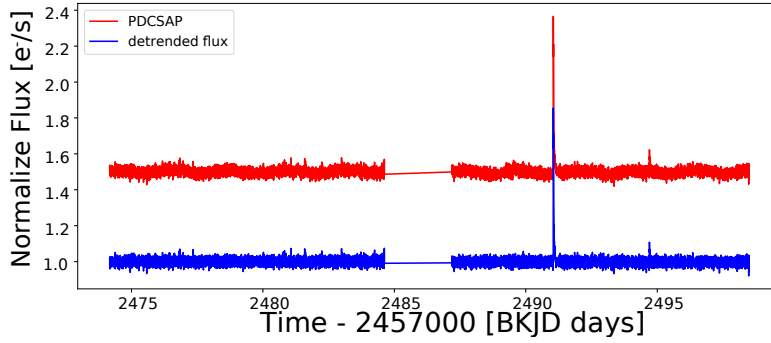


Figure 3: PDCSAP and detrended light curves of MHO 4 for sector 44. The x -axis represents time, in Barycentric Kepler Julian Days (BKJD), and the y -axis represents the normalized TESS flux (e^-/s). PDCSAP data are shown in red and the detrended flux (e^-/s) with no intrinsic variation present is displayed in blue.

3.1. Flare detection and analysis

As a result of flare detection, we have identified one flare from each sector of MHO 4. As an example, we present the PDCSAP and detrended light curve for sector 44 in Fig. 3.

Initially, we visually inspected and confirmed the detection of flares by the open source *Python* software *AltaiPony* (Ilin, 2021). This software provides several flare parameters, such as, e.g., start and stop time, flare amplitude, and equivalent duration (ED). To estimate the bolometric flare energy, we used the equation defined by Shibayama et al. (2013) and Ikuta et al. (2023). Assuming the flare as a blackbody of temperature 10,000 K, we calculated the flare energy as 4.01×10^{34} erg in sector 43 and 1.59×10^{35} erg in sector 44. Table 1 describes the details of the flare parameters.

Generally, flare light curves in BDs exhibit a rapid rise and gradual decline in brightness. However, all flare light curves show multi-peaked behavior in the decline phase, suggesting that

Table 1: Details of flare properties of MHO 4. The radius (Radius) and temperature (Temp) are taken from Stassun et al. (2018) while the relative amplitude (Rel Amp) and equivalent duration (ED) were computed using the AltaiPony software.

Object	Sector	Radius (R_{Sun})	Temp (K)	Rel Amp	ED (s)	Energy (erg)	Duration (min)
MHO 4	43	0.655	2814.0	0.857	1479.79 ± 11.10	4.01×10^{34}	84
	44	0.655	2814.0	1.209	5852.15 ± 22.17	1.59×10^{35}	298

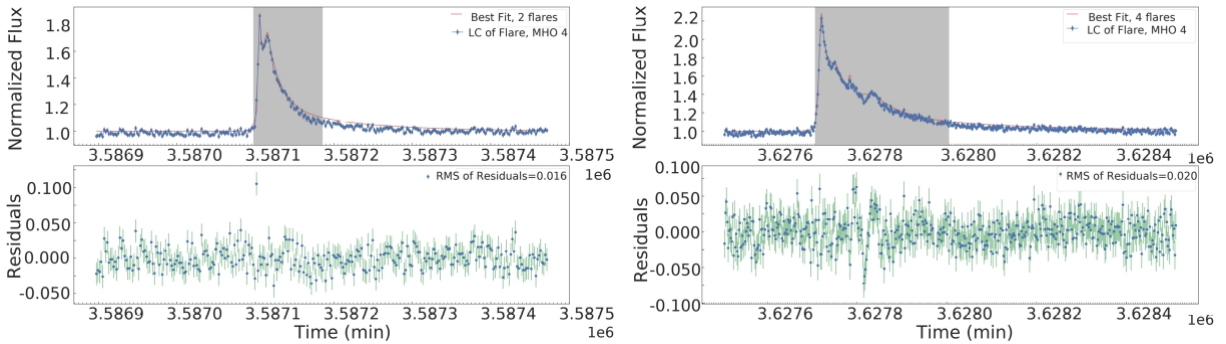


Figure 4: (Top) Model-fitted flare light curve of MHO 4 in sector 43 (left) and sector 44 (right) using *Allesfitter*. Blue points represent TESS 2-min observational cadence data, and the red line denotes the best-fitted curve. The x -axis represents time in minutes, the y -axis the PDCSAP flux. The grey area indicates the region of the duration of flares. (Bottom) RMS values of the residuals of the fitted light curves.

such flare events are complex. We further analyzed and modeled these flare light curves using open-source package *Allesfitter* (Günther and Daylan, 2021). We modeled the flare light curve using the Nested Sampling algorithm (Skilling, 2006), which provides the flares' peak times, amplitudes and FWHMs, white noise scaling, and a constant baseline. As a preliminary result, we found two flare candidate peaks in sector 43, whereas in sector 44, four flare candidate peaks fitted well to the flares. Figure 4 illustrates the fitted flare light curves and their residuals. Figure 5 shows the posterior probability distribution of the flare parameters.

Inspecting the power spectrum and phase light curve of MHO 4, we identified a significant peak in the LS periodogram. Folding the light curve at this period revealed a clear, smooth variation across the different sectors. Such smooth variations are typically associated with rotational modulation mainly of the spots or groups of spots with the objects (Rebull et al., 2016). So, here we deduced the mean spot temperature T_{spot} of MHO 4 using a quadratic formula proposed by Herbst et al. (2021):

$$T_{\text{spot}} = -3.58 \times 10^{-5} T_{\text{eff}}^2 + 0.801 \times T_{\text{eff}} + 666.5$$

Additionally, we illustrated the spot relative intensity f_{spot} for the TESS band, which depends

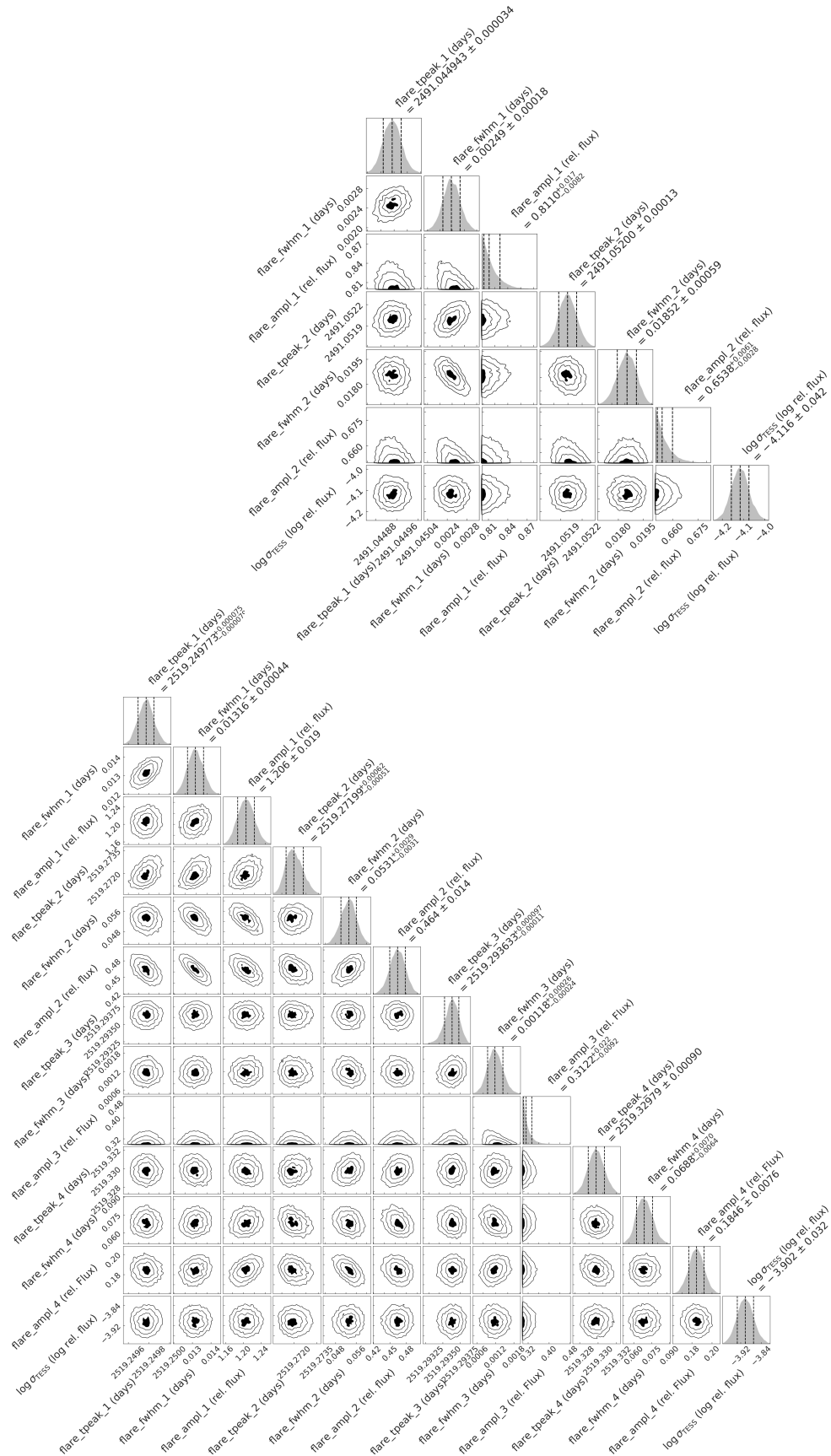


Figure 5: Posterior probability distributions of the flare parameters in the light curve model for sector 43 (*top*) and sector 44 (*bottom*).

on the stellar effective temperature T_{eff} and the spot temperature, T_{spot} :

$$f_{\text{spot}} = \frac{\int R_{\lambda} B_{\lambda}(T_{\text{spot}}) d\lambda}{\int R_{\lambda} B_{\lambda}(T_{\text{eff}}) d\lambda}.$$

By applying these equations, we estimated the mean spot temperature of MHO 4 to be approximately 2638 K, with a spot relative intensity of approximately 0.65.

4. Summary

In this work, we investigated the photometric variability of a young brown dwarf (BD) in the Taurus region, MHO 4, using 2-min cadence data from TESS to search for its rotation periods and atmospheric properties. Our analysis revealed a rotation period of approximately 2.224 d for MHO 4, with its phase light curve showing smooth variations indicative of rotational modulation due to asymmetrically distributed starspots or groups of spots on its surface. We used two independent techniques, the Lomb–Scargle periodogram and the Gaussian Process method, to determine the rotation period, both yielding consistent results. In addition, we identified two superflare events from MHO 4, with estimated bolometric energies of 4.01×10^{34} erg (sector 43) and 1.59×10^{35} erg (sector 44). Finally, to model the flare light curves, we observed that the flare in sector 43 was fitted with two flare candidate peaks, while four flare candidate peaks were required to fit well in sector 44.

Acknowledgments

We would like to thank Dr. Priya Hasan, whose valuable comments and suggestions helped to improve the manuscript. This research work is supported by the S. N. Bose National Centre For Basic Sciences under the Department of Science and Technology, Govt. of India. This study uses TESS mission data retrieved from the Space Telescope Science Institute (STScI). RK is grateful to the Department of Science and Technology (DST), Govt. of India, for their support through the INSPIRE Fellowship scheme.

Further Information

Authors' ORCID identifiers

0000-0001-7277-2577 (Rajib KUMBHAKAR)

0000-0003-1457-0541 (Soumen MONDAL)

0000-0003-3354-850X (Samrat GHOSH)

0009-0008-7884-3741 (Diya RAM)

Author contributions

The light curves and power spectrum analysis were carried out by RK, SM and SG. The examination of the flare analysis part was performed by SG and RK. The text was written by RK. All of the authors provided input on the written draft of the manuscript as well as the discussion and interpretation of the findings.

Conflicts of interest

The authors declare no conflict of interest.

References

- Angus, R., Morton, T., Aigrain, S., Foreman-Mackey, D. and Rajpaul, V. (2018) Inferring probabilistic stellar rotation periods using Gaussian processes. *MNRAS*, 474(2), 2094–2108. <https://doi.org/10.1093/mnras/stx2109>.
- Baglin, A., Auvergne, M., Boisnard, L., Lam-Trong, T., Barge, P., Catala, C., Deleuil, M., Michel, E. and Weiss, W. (2006) CoRoT: a high precision photometer for stellar evolution and exoplanet finding. *COSPAR Scientific Assembly*, 36, 3749.
- Briceño, C., Hartmann, L., Stauffer, J. and Martín, E. (1998) A search for very low mass pre-main-sequence stars in Taurus. *AJ*, 115(5), 2074–2091. <https://doi.org/10.1086/300338>.
- Carnero Rosell, A., Santiago, B., dal Ponte, M., Burningham, B., da Costa, L. N., James, D. J., Marshall, J. L., McMahan, R. G., Bechtol, K., De Paris, L., Li, T., Pieres, A., García-Bellido, J., Abbott, T. M. C., Annis, J., Avila, S., Bernstein, G. M., Brooks, D., Burke, D. L., Carrasco Kind, M., Carretero, J., De Vicente, J., Drlica-Wagner, A., Fosalba, P., Frieman, J., Gaztanaga, E., Gruendl, R. A., Gschwend, J., Gutierrez, G., Hollowood, D. L., Maia, M. A. G., Menanteau, F., Miquel, R., Plazas, A. A., Roodman, A., Sanchez, E., Scarpine, V., Schindler, R., Serrano, S., Sevilla-Noarbe, I., Smith, M., Sobreira, F., Soares-Santos, M., Suchyta, E., Swanson, M. E. C., Tarle, G., Vikram, V., Walker, A. R. and DES Collaboration (2019) Brown dwarf census with the Dark Energy Survey year 3 data and the thin disc scale height of early L types. *MNRAS*, 489(4), 5301–5325. <https://doi.org/10.1093/mnras/stz2398>.
- Carpenter, J. M., Hillenbrand, L. A. and Skrutskie, M. F. (2001) Near-infrared photometric variability of stars toward the Orion A molecular cloud. *AJ*, 121(6), 3160–3190. <https://doi.org/10.1086/321086>.
- Foreman-Mackey, D. (2018) Scalable backpropagation for Gaussian Processes using celerite. *RNAAS*, 2(1), 31. <https://doi.org/10.3847/2515-5172/aaaf6c>.
- Foreman-Mackey, D., Luger, R., Agol, E., Barclay, T., Bouma, L., Brandt, T., Czekala, I., David, T., Dong, J., Gilbert, E., Gordon, T., Hedges, C., Hey, D., Morris, B., Price-Whelan, A. and Savel, A. (2021) *exoplanet*: Gradient-based probabilistic inference for exoplanet

- data & other astronomical time series. *JOSS*, 6(62), 3285. <https://doi.org/10.21105/joss.03285>.
- Ghosh, S., Mondal, S., Dutta, S., Das, R., Joshi, S., Lata, S., Khata, D. and Panja, A. (2021) Fast photometric variability of very low mass stars in IC 348: detection of superflare in an M dwarf. *MNRAS*, 500(4), 5106–5116. <https://doi.org/10.1093/mnras/staa3574>.
- Güdel, M., Briggs, K. R., Arzner, K., Audard, M., Bouvier, J., Feigelson, E. D., Franciosini, E., Glauser, A., Grosso, N., Micela, G., Monin, J. L., Montmerle, T., Padgett, D. L., Palla, F., Pillitteri, I., Rebull, L., Scelsi, L., Silva, B., Skinner, S. L., Stelzer, B. and Telleschi, A. (2007) The XMM–Newton extended survey of the Taurus molecular cloud (XEST). *A&A*, 468(2), 353–377. <https://doi.org/10.1051/0004-6361:20065724>.
- Günther, M. N. and Daylan, T. (2021) Allesfitter: Flexible star and exoplanet inference from photometry and radial velocity. *ApJS*, 254(1), 13. <https://doi.org/10.3847/1538-4365/abe70e>.
- Herbst, K., Papaioannou, A., Airapetian, V. S. and Atri, D. (2021) From starspots to stellar coronal mass ejections—Revisiting empirical stellar relations. *ApJ*, 907(2), 89. <https://doi.org/10.3847/1538-4357/abcc04>.
- Howell, S. B., Sobeck, C., Haas, M., Still, M., Barclay, T., Mullally, F., Troeltzsch, J., Aigrain, S., Bryson, S. T., Caldwell, D., Chaplin, W. J., Cochran, W. D., Huber, D., Marcy, G. W., Miglio, A., Najita, J. R., Smith, M., Twicken, J. D. and Fortney, J. J. (2014) The K2 mission: Characterization and early results. *PASP*, 126(938), 398. <https://doi.org/10.1086/676406>.
- Ikuta, K., Namekata, K., Notsu, Y., Maehara, H., Okamoto, S., Honda, S., Nogami, D. and Shibata, K. (2023) Starspot mapping with adaptive parallel tempering. II. Application to TESS data for M-dwarf flare stars AU Microscopii, YZ Canis Minoris, and EV Lacertae. *ApJ*, 948(1), 64. <https://doi.org/10.3847/1538-4357/acbd36>.
- Ilin, E. (2021) AltaiPony – Flare science in Kepler, K2 and TESS light curves. *JOSS*, 6(62), 2845. <https://doi.org/10.21105/joss.02845>.
- Jenkins, J. M., Twicken, J. D., McCauliff, S., Campbell, J., Sanderfer, D., Lung, D., Mansouri-Samani, M., Girouard, F., Tenenbaum, P., Klaus, T., Smith, J. C., Caldwell, D. A., Chacon, A. D., Henze, C., Heiges, C., Latham, D. W., Morgan, E., Swade, D., Rinehart, S. and Vanderspek, R. (2016) The TESS science processing operations center. *SPIE*, 9913, 3E. <https://doi.org/10.1117/12.2233418>.
- Joergens, V. (2014) The theoretical prediction of the existence of brown dwarfs by Shiv S. Kumar. *ASSL*, 401, 1. https://doi.org/10.1007/978-3-319-01162-2_1.
- Lightkurve Collaboration, Cardoso, J. V. d. M., Hedges, C., Gully-Santiago, M., Saunders, N., Cody, A. M., Barclay, T., Hall, O., Sagar, S., Turtelboom, E., Zhang, J., Tzanidakis, A., Mighell, K., Coughlin, J., Bell, K., Berta-Thompson, Z., Williams, P., Dotson, J. and Bar-entsen, G. (2018) Lightkurve: Kepler and TESS time series analysis in Python. *Astrophysics Source Code Library*, record ascl:1812.013.

- Martín, E. L., Delfosse, X., Basri, G., Goldman, B., Forveille, T. and Zapatero Osorio, M. R. (1999) Spectroscopic classification of late-M and L field dwarfs. *AJ*, 118(5), 2466–2482. <https://doi.org/10.1086/301107>.
- Matthews, J. M., Kuschnig, R., Walker, G. A. H., Pazder, J., Johnson, R., Skaret, K., Shkolnik, E., Lanting, T., Morgan, J. P. and Sidhu, S. (2000) Ultraprecise photometry from space: The MOST microsat mission. In *IAU Colloq. 176: The Impact of Large-Scale Surveys on Pulsating Star Research*, edited by Szabados, L. and Kurtz, D., vol. 203, pp. 74–75. <https://ui.adsabs.harvard.edu/abs/2000ASPC..203...74M/abstract>.
- Rebull, L. M., Stauffer, J. R., Bouvier, J., Cody, A. M., Hillenbrand, L. A., Soderblom, D. R., Valenti, J., Barrado, D., Bouy, H., Ciardi, D., Pinsonneault, M., Stassun, K., Micela, G., Aigrain, S., Vrba, F., Somers, G., Christiansen, J., Gillen, E. and Collier Cameron, A. (2016) Rotation in the Pleiades with K2. I. Data and first results. *AJ*, 152(5), 113. <https://doi.org/10.3847/0004-6256/152/5/113>.
- Rebull, L. M., Stauffer, J. R., Cody, A. M., Hillenbrand, L. A., Bouvier, J., Roggero, N. and David, T. J. (2020) Rotation of low-mass stars in Taurus with K2. *AJ*, 159(6), 273. <https://doi.org/10.3847/1538-3881/ab893c>.
- Ricker, G. R., Winn, J. N., Vanderspek, R., Latham, D. W., Bakos, G. Á., Bean, J. L., Berta-Thompson, Z. K., Brown, T. M., Buchhave, L., Butler, N. R., Butler, R. P., Chaplin, W. J., Charbonneau, D., Christensen-Dalsgaard, J., Clampin, M., Deming, D., Doty, J., De Lee, N., Dressing, C., Dunham, E. W., Endl, M., Fressin, F., Ge, J., Henning, T., Holman, M. J., Howard, A. W., Ida, S., Jenkins, J. M., Jernigan, G., Johnson, J. A., Kaltenegger, L., Kawai, N., Kjeldsen, H., Laughlin, G., Levine, A. M., Lin, D., Lissauer, J. J., MacQueen, P., Marcy, G., McCullough, P. R., Morton, T. D., Narita, N., Paegert, M., Palle, E., Pepe, F., Pepper, J., Quirrenbach, A., Rinehart, S. A., Sasselov, D., Sato, B., Seager, S., Sozzetti, A., Stassun, K. G., Sullivan, P., Szentgyorgyi, A., Torres, G., Udry, S. and Villaseñor, J. (2015) Transiting Exoplanet Survey Satellite (TESS). *JATIS*, 1, 014003. <https://doi.org/10.1117/1.JATIS.1.1.014003>.
- Shibayama, T., Maehara, H., Notsu, S., Notsu, Y., Nagao, T., Honda, S., Ishii, T. T., Nogami, D. and Shibata, K. (2013) Superflares on solar-type stars observed with *Kepler*. I. Statistical properties of superflares. *ApJS*, 209(1), 5. <https://doi.org/10.1088/0067-0049/209/1/5>.
- Skilling, J. (2006) Nested sampling for general Bayesian computation. *BayAn*, 1, 833–860. <https://doi.org/10.1214/06-BA127>.
- Stassun, K. G., Oelkers, R. J., Pepper, J., Paegert, M., De Lee, N., Torres, G., Latham, D. W., Charpinet, S., Dressing, C. D., Huber, D., Kane, S. R., Lépine, S., Mann, A., Muirhead, P. S., Rojas-Ayala, B., Silvotti, R., Fleming, S. W., Levine, A. and Plavchan, P. (2018) The TESS Input Catalog and Candidate Target List. *AJ*, 156(3), 102. <https://doi.org/10.3847/1538-3881/aad050>.

- VanderPlas, J. T. (2018) Understanding the Lomb–Scargle periodogram. *ApJS*, 236(1), 16. <https://doi.org/10.3847/1538-4365/aab766>.
- Wang, X.-L., Fang, M., Herczeg, G. J., Gao, Y., Tian, H.-J., Zhou, X.-Y., Zhang, H.-X. and Chen, X.-P. (2023) Variability of young stellar objects in the Perseus molecular cloud. *RAA*, 23(7), 075015. <https://doi.org/10.1088/1674-4527/acd58b>.
- White, R. J. and Basri, G. (2003) Very low mass stars and brown dwarfs in Taurus–Auriga. *ApJ*, 582(2), 1109–1122. <https://doi.org/10.1086/344673>.